



BEAMFORMING AND DECONVOLUTION FOR AERODYNAMIC SOUND SOURCES IN MOTION

Sébastien Guérin, Christian Weckmüller, Ulf Michel

Deutsches Zentrum für Luft- und Raumfahrt
Müller-Breslau-Str. 8, 10623, Berlin, Germany

ABSTRACT

Acoustic beamforming with microphone phased-arrays is a powerful method to investigate the noise emission of vehicles (aircraft, trains, cars, etc.). Per definition, the aerodynamic sound sources appear when these vehicles are in motion. Some of the sources, like the high-lift devices of aircraft, are distributed in space.

The beamforming patterns are the result of a convolution between the sources and point spread functions, which depend on the array geometry and source position. The performance of a phased array is characterised by two parameters: i) the beamwidth on which depends the capacity to separate two sources close to each other, and ii) the level of the side-lobes which describes the dynamic range. In static applications (the source positions are fixed with respect to the microphone array) the source strength of distributed sources can be determined by deconvoluting the beamforming solution. Some issues arise when a deconvolution is applied to moving sources because the frequencies of the side-lobes are shifted with respect to the main lobe. An approximate method for the deconvolution of the beampattern of moving broadband sources is derived and it is shown with simulated data that solutions can be obtained with a reasonable accuracy and computing time.

1 INTRODUCTION

The acoustic beamforming technique has been largely used in aeronautics to investigate and characterise aerodynamic noise (jet noise [1], airframe noise [2], etc.). It has even been employed to identify aircraft wake vortices [3]. Very recent developments deals with the source localisation in fan ducts [4]. The present paper concerns the application of beamforming to aircraft in flyover [5]. Beamforming has made it possible to locate unexpected acoustic sources like cavity tones and thus contributed to reduce the airframe noise component of modern aircraft. New objectives have been defined to improve the method in order to assess individually the acoustic strengths of the different airframe components (landing gear, slats, flaps, etc.).

Beamforming can either be formulated in the time domain or in the frequency domain. In the time domain the microphone signals are delayed and summed whereas in the frequency domain the cross-spectrum matrix of the microphone signals is multiplied by a steering vector. Static measurements (typically wind tunnel tests) are usually treated in the frequency domain since the computation is quicker. For stationary random sources, the time domain solution should come to the same results. Measurements in which the source is in motion

relative to the microphone array (for instance aircraft flyover tests) are treated only in the time domain. In these cases, the frequency perceived by each microphone installed on the ground is continuously changing with time due to the Doppler effect; therefore no correlation at the same frequency can be built between the different microphone signals.

Since the beamforming patterns result from a convolution between the sources and the associated point spread functions, the absolute level of distributed sources cannot be directly assessed. Two methods have recently been proposed to find a solution for this problem. The first method, described by Brooks and Humphreys [6], consists of deconvoluting the beamforming results. The second method, proposed by Blacodon and Elias [7], minimizes the error between the measured and the modelled cross-spectrum matrices. Since the method works with the cross-spectrum matrix of the microphone signals the spectral analysis cannot be applied to moving sources. Another limitation is the size of the problem to solve: its dimension is M^2 higher than for beamforming deconvolution (with M the number of microphones). An ideal way to solve the deconvolution problem with moving sources would be to compute the point spread function in the time domain and minimize the error in the frequency domain simultaneously over the complete frequency range. But the calculation of the point spread function in the time domain for all focusing points is alone not affordable in terms of computing time.

The method presented here is a hybrid one: the beamforming results are calculated in the time domain and the point spread function is approximated in the frequency domain taking into account an average Doppler frequency shift. This method can be considered as a simplification of what Brühl and Röder presented [8] with the difference that the frequency coupling is discarded from the formulation. There are several reasons to do so. First it is not possible to take properly into account the frequency coupling since realistically only the nearest frequency band can be selected and second it increases dramatically the size of the problem to solve. Furthermore the broadband aerodynamic sources characterized by a flat spectrum have interesting features that should exempt from taking into account explicitly the frequency shift on the side-lobes. In the present paper, the accuracy of our method is assessed with synthesized data.

2 BEAMFORMING

2.1 Time domain formulation

The formulation for the beamforming time solution b is given by

$$b(t) = \sum_{m=1}^M \frac{r_m}{r_{ref}} w_m p_m(t + r_m / c_0) \quad (1)$$

where p_m is the de-dopplerized signal of the m^{th} microphone, t the emission time, r_m the distance between the microphone and the focusing point, r_{ref} a distance for normalization, w_m a weighting factor that satisfies Eq. 2, M the number of microphones, and c_0 the speed of sound. Eq. 1 is a simple “delay and sum” operation. With moving sources, the distance r_m is time dependent and must be evaluated at every time step t .

$$\sum_{m=1}^M w_m = 1 \quad (2)$$

The result from Eq. 1 can be then represented in the frequency domain by Fourier transforming the solution.

2.2 Frequency domain formulation (static sources)

The pressure emitted by a harmonic monopole point source at rest is

$$p_m(t) = \frac{A}{r_m} e^{-i\omega(t-r_m/c_0)} \quad (3)$$

where A is the source amplitude and ω the radian frequency.

An equivalent formulation of Eq. 1 in the frequency domain is

$$\mathbf{B} = \mathbf{S}^T \mathbf{W} \mathbf{G} \mathbf{W}^T \mathbf{S} \quad (4)$$

In Eq. 4, \mathbf{G}_{mn} represents the cross-spectrum matrix of the microphone signals defined by

$$\mathbf{G}_{mn}(\omega) = \langle \mathbf{c}_m^*(\omega) \mathbf{c}_n(\omega) \rangle \quad (5)$$

where $\langle \rangle$ denotes an averaging over a number of FFT blocks, \mathbf{c} the Fourier transform of the microphone pressure signal, and $*$ the complex conjugate. The steering vector \mathbf{S} has also been introduced with element

$$S_m = \frac{r_m}{r_{ref}} e^{-ikr_m} \quad (6)$$

where $k = \omega/c_0$ is the wave number. The diagonal matrix \mathbf{W} contains the weighting factors applied to the microphones ($Tr(\mathbf{W}) = 1$).

2.3 Frequency shift on side-lobes with moving sources

The Doppler factor Df is defined by

$$Df = \frac{1}{1 - M_0 \cos \mathbf{q}} \quad (7)$$

where $M_0 = U/c_0$ is the Mach number and \mathbf{q} the angle of emission $\mathbf{q} = 0$ in the direction of motion. Because of the Doppler effect the side-lobes produced by beamforming are frequency shifted compared to the source. For a source S of frequency ω_s at position \vec{x}_s , the frequency ω_F at focused point F at \vec{x}_F is

$$\begin{aligned} \omega_F &= \omega_s \frac{Df_s}{Df_F} = \frac{1 - M_0 \cos \mathbf{q}_F}{1 - M_0 \cos \mathbf{q}_S} \\ \text{with } \cos \mathbf{q}_S &= \frac{-\vec{x}_s \cdot \vec{U}}{\|\vec{x}_s\| \cdot \|\vec{U}\|} \\ \cos \mathbf{q}_F &= \frac{-\vec{x}_F \cdot \vec{U}}{\|\vec{x}_F\| \cdot \|\vec{U}\|} \end{aligned} \quad (8)$$

This effect is shown in Fig. 1 where a simulation conducted with a point source at rest ($U = 0$ m/s) is compared to another simulation performed with a point source moving with a speed of $U = 80$ m/s. The source in both cases is harmonic of frequency 1 kHz and emits sound from an altitude of 200 m. The array is a one-dimensional array composed of 101 microphones separated by 0.15 m. The calculations were performed in the time domain. The x -axis represents the focusing domain of 60 m aperture in the middle of which is the source. The y -axis represents the non-dimensional frequency ω/ω_s . While the energy of the side-lobes is contained at the original frequency in the static case, we observe with motion that the side-lobes are frequency shifted. The maximal frequency shift is found for the two extremities of the focusing domain, i.e. for the points E ($x = -30$ m) and G ($x = +30$ m). In Fig. 2 the instantaneous Doppler factor ratio Df/Df_{FC} for these two extremities E and G relative to the array centre C is represented as a function of emission angle. The values at 60° , 90° and 120°

correspond to the values obtained by the simulations shown in Fig. 1. It can be seen that the frequency shift of the side-lobes is largest for the emission angle of 90°, when the aircraft is overhead at emission time. The maximum shift amounts to 3.5%. In the simulations presented later the frequency step of the Fast Fourier Transform is 25 Hz. This corresponds to 10% at 250 Hz, 2.5% at 1000 Hz and 1% at 2500 Hz. The side-lobes of a source in the centre are still contained in the same frequency band at 250 Hz, when the beamform map is computed for the two extremities. However, at 1000 Hz, the frequencies of the sidelobes span over three neighbouring frequency bands. At 2500 Hz the sidelobes would span a total of 7 frequency bands. The number of frequency bands is proportional to the frequency and inversely proportional to the frequency step of the analysis.

3 DECONVOLUTION OF BEAMFORMING

3.1 Static sources

For aerodynamic sources, the square amplitude $\mathbf{s} = A^2$ of a set of I monopoles modelling the source region can be restored from the output B of classical beamforming by solving the following non-negative least square problem

$$C(A) = \sum_{i=1}^I \left(\sum_{j=1}^I H_{ij} \mathbf{s}_j - B_i \right)^2 \quad (9)$$

$$\mathbf{s}_i \geq 0$$

where H is the matrix of the point spread functions defines by

$$H_{ij}(\mathbf{w}) = \left(\sum_{m=1}^M w_m \frac{r_{mj}}{r_{mi}} e^{-ik(r_{mi}-r_{mj})} \right)^2 \quad (10)$$

The subscript i and j correspond to the focusing point and the source position, respectively. Thus a column $(H_{1j} \dots H_{Ij})$ represents the beamforming pattern for a monopole of amplitude 1 at position j .

In Eq. 9 the constraint accounts for the fact that the amplitude of each source must be positive. Several iterative methods have been proposed to solve this equation and speed up the computation [6], [9], and [10]. In the present paper the modified Gauss-Seidel method presented in [6] is used. This method contains no regularization technique to prevent noise amplification. However it converges quickly towards a very acceptable solution as will be shown hereafter.

Typically for mapping an aircraft in flyover, a grid of $I=100 \times 100$ points is necessary. It follows that H is a 10000 \times 10000 matrix. The construction of this matrix for every frequency can represent a very significant part of the computation time. However this effort can be dramatically reduced by assuming that the matrix is translationally-invariant over a certain angle of aperture which limits the number of point spread functions to calculate [9]. In the present paper, the size of the mesh was fixed to $I=75 \times 75$ points hence a 5625 \times 5625 H -matrix. The latter was constructed whereas only 144 source positions were actually calculated.

3.2 Moving sources

The pressure emitted by a moving point source with an angular frequency \mathbf{w} is received by a microphone with a Doppler shift.

$$p_m^M(t) = A \frac{C(t)}{r_m(t)} e^{i\mathbf{w}Df(t)(t-r_m(t)/c_0)} \quad (11)$$

where C is a convective amplification factor (not considered here) and $Df(t)$ the Doppler frequency shift. Thus each microphone perceives a signal with a different frequency at every time t .

The ideal way to solve the deconvolution problem would be to compute the point spread functions in the time domain and minimize the cost function in Eq. 9 over all the frequency lines simultaneously. But the calculation of the point spread functions in the time domain for the whole scanning area is alone not affordable in terms of computing time.

Instead we propose to calculate the point spread function with the following formula

$$H_{ij}^M(\mathbf{w}) = \left(\sum_{m=1}^M w_m \frac{r_{mj}}{r_{mi}} e^{-ikDf(r_{mi}-r_{mj})} \right)^2 \quad (12)$$

where an average Doppler frequency shift calculated between the centre of the focusing domain and the array centre is introduced. With broadband sources having a flat spectrum, energy is exchanged between the different frequency bands. At the end it is expected that the difference between the ideal point spread function and the modelled one remains acceptable. Tones would have to be studied separately.

4 RESULTS

4.1 Simulations

The simulations were conducted for an array designed for a series of flyover tests that took place in Parchim in 2004 [11], [12]. These tests performed with a Lufthansa operated A319 aircraft were carried out within the framework of the German project LAnAb, co-financed by the Federal Ministry of Education and Research. The array consisted of 168 microphones distributed in 7 spirals with a logarithmic radial spacing. The properties of this array (beamwidth and side-lobe rejection) are provided in Fig. 3 after shading. The average flyover altitude, 200 m, and groundspeed, about $U = 80$ m/s, were used as parameters for the simulations. The size of the focusing domain $37 \text{ m} \times 37 \text{ m}$ is slightly larger than the aircraft size, whose wingspan is 34 m.

Five source configurations were investigated (see Table 1). Every configuration was simulated at negligible speed 0.1 m/s (viewed as a way to introduce some distortion) and at 80 m/s. Only the results for the S1/S1M and S5/S5M configurations are presented here. They refer, respectively, to simulations performed with a single point source in the centre of the focusing domain, and 546 incoherent sources with identical amplitudes. In the latter configuration the sources are arranged equidistantly along lines that simulate the flaps and slats of an A319 aircraft.

All individual point sources are stationary random in nature and generated with an original sampling frequency f_s . For the need of beamforming the microphone signals were resampled at lower frequency f_{res} . According to the sampling theory the part of the spectrum between $f_{res}/2$ and $f_s/2$ is mirrored. With the present simulations the energy contained in the original signal drops significantly above the resampling frequency $f_{res}/2$ despite no low-filtering technique was employed (see Fig. 4). Thus up to frequency $f_{res}/4$ the presence of spectral aliases can not be suspected. The small variations observed between neighbouring frequency bands are inherent to the relative short time length used to compute the spectrum and are function of the processing parameters (signal duration, FFT size, FFT window, etc.). Many of the aircraft aerodynamic sound sources have a strong directivity which implies that only short durations of flight are considered for each emission angle \mathbf{q} . In the following the aperture angle was fixed to $\Delta\mathbf{q} = 12^\circ$ for the simulations with motion which corresponds to ~ 0.5 s at $\mathbf{q} = 90^\circ$, $U = 80$ m/s and $h = 200$ m. The same duration was considered for the

static simulations. When not mentioned in the text, the processing parameters given in Table 2 were used.

Table 1. Simulated test cases.

Source conf.	ID	Speed of motion	Number of sources
Point source	S1/S1M	0.1/80 m/s	1
Landing gear	S2/S2M	0.1/80 m/s	3
2 Engines	S3/S3M	0.1/80 m/s	6
Slats	S4/S4M	0.1/80 m/s	282
Slats and Flaps	S5/S5M	0.1/80 m/s	546

Table 2. Processing parameters.

Sampling frequency	48192 Hz
Resampling frequency	25600 Hz
Time length	~0.5 s
FFT size	1024
FFT window	Hanning
Mesh size, $N_x \times N_y$	75×75
Spatial resolution, $\Delta x \times \Delta y$	$0.5 \text{ m} \times 0.5 \text{ m}$

4.2 Point source cases S1/S1M

One objective of the test case 1 was to compare the time domain solution CBF calculated with Eq. 1 and the point spread function $H_{is} = (H_{1s} \dots H_{Is})$ for the source. Ideally the two results should be identical in the static case. A comparison is shown in Fig. 5 for two representative frequencies 250 Hz and 1 kHz with the source at the vertical of the array centre ($\mathbf{q} = 90^\circ$). This comparison was done for a 37×37 mesh with $1 \text{ m} \times 1 \text{ m}$ resolution. The normalized difference

$$err = \frac{\|CBF - H_{is}\|}{\|H_{is}\|} \quad (13)$$

at 250 Hz and 1 kHz is 0.54% and 0.19%, respectively. This means a very good agreement between the modelled point spread function and the calculations. The highest discrepancies are found between the side-lobes where minima are occurring. Whereas a null value can be reached between two side-lobes with the point spread function, the levels obtained by beamforming seem to be not able to drop below a certain value. The reason is that the re-sampling of the original microphone signals introduces noise in the beamforming solution. The small source motion and the interpolation of the point spread function may also accentuate the difference. In Fig. 6 the same comparison is done for the case S1M with motion. The difference is now 1.59% and 1.37% at 250 Hz and 1 kHz, respectively. Compared to S1, the error has increased as expected but remains small. Two reasons may explain this good result. First the analysis is made with a frequency bandwidth of 25 Hz. Thus the energy contained by the side-lobes remains within the same frequency band when it is multiplied by the Doppler frequency ratio. But this effect disappears at high frequencies. The other reason concerns the transfer of energy between the frequency bands and can be formulated as follows for a source with a flat spectrum: the energy lost per one band because of the frequency shift on the side-lobes is compensated by the energy received from the other frequency bands.

The same kind of evaluation was done at 60° . Beamforming and modelled point spread function can be visualized in Fig. 7 and 8. For S1 and S1M the error is 2.01% / 7.33% and

8.73% / 9.07% at 250 / 1000 Hz, respectively. Thus the error is significantly higher at 60° than 90° which may be due to the interpolation of the point spread function. On the other hand the difference between the static and moving cases remains reasonable. In Fig. 9 this difference is plotted for a series of frequencies between 200 Hz and 5 kHz.

The procedure is now applied to the deconvolution problem. In Fig. 10 and 11 the results from beamforming and deconvolution are compared in one third octave bands for $\mathbf{q} = 90^\circ$ and 60°. After deconvolution the large beam is replaced by one or several elementary sources located very close to the original source position. The number of these elementary sources drops when the beamwidth decreases. Apparently the source motion does not significantly deteriorate the deconvolution results. The normalized residual from the calculation defined by

$$residual = \frac{\|HA - B\|}{\|B\|} \quad (14)$$

are provided in Fig. 12. In the best case (S1 at 90°) the residuals are of the order of 1% whereas in the worst case (S1M at 60°) they are of the order of 10% which may seem not satisfactory. Note that small residuals were obtained with the source S1 at rest although the number of iterations was limited to a maximum number of 100 with a minimum of 20 (see Fig. 13).

Another way to assess the quality of the method is to compare the original source spectrum to the reconstructed one. The original source spectrum is given by the de-dopplerized spectrum [12], whereas the reconstructed spectrum is obtained by integrating (summing) the deconvolution solution over a small area around the source. In the present case a square of 1 m by 1 m centred on the source was chosen as integration surface. This represents exactly 25 points for a total number of 5625, i.e. 0.44% of the focusing area. The results presented in Fig 14 show a very good agreement between the source and the reconstructed spectra. The difference is actually less than 0.5 dB over the almost complete frequency range for both the static and the moving cases. The noise level calculated with the points outside of the source area (i.e. 99.56% of the total focusing plane) is in average 15 dB below the source level for the non-moving case and 10 dB with motion. These are values which indicate that the problem has been solved with a sufficient accuracy even though the level of the residuals may be high.

4.3 Distributed source cases S5/S5M

The test case 5 simulates distributed sources located at the slats and flaps of the aircraft (see Fig. 15). The slats and flaps are represented by 282 and 264 point sources respectively. All the point sources have the same level and are stationary random. The comparison beamforming/deconvolution is shown in Fig 16 for $\mathbf{q} = 90^\circ$. While the line sources at the slats and flaps cannot be distinguished with beamforming, they are well separated after deconvolution. The reason why the results look better at high than at low frequency is principally statistical, because the one-third octave bands contain more narrow-band frequency bands for higher frequencies. The residuals (see Fig. 17) from the iterative solution are very close for the static and the moving cases and less than 10%. We can also observe that the residual levels jump at the border between two one-third octave bands. This is due to the shading function which is different for every one-third octave band. This demonstrates that the beamforming properties (beamwidth and side-lobe rejection) are influencing the solution. The spectrum level of the reconstructed source is compared to the total spectrum in Fig 18. The integration surface is defined in Fig. 19 and represents 4.5% of the total focusing area. Again there is a very good agreement between both spectra. Furthermore the reconstructed spectra for the flaps and the slats are very similar which is correct since both sources have about the same number of point sources hence the same amplitude. With an average value of 12 dB signal-to-noise ratio the static solution is slightly less noisy than the moving solution.

5 CONCLUSION

A deconvolution method of beamforming maps for moving broadband sources has been formulated and applied to synthesized data. The calculations, performed with the pro Σ C++-program developed at the Institute of Propulsion Technology of DLR in Berlin show:

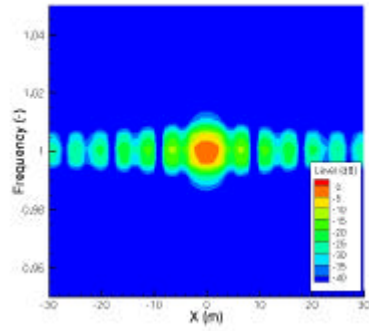
- Using a frequency domain formulation, it is possible to reproduce the point spread function in the time domain accurate enough despite the errors introduced by interpolation and statistical uncertainties.
- When the source is moving there is a frequency shift between the main lobe and the side-lobes. Assuming the source has a flat spectrum (which is the case for most of the aerodynamic sources); there is an inter-frequency band exchange of beamforming energy. The deconvolution problem can then be solved by taking into account an average Doppler shift.
- The level of the modified Gauss-Seidel method used to solve the deconvolution problem is an indicator of the background noise. With 10% residual very satisfactory results were obtained since the source was resolved with 0.5 dB and 10 dB signal-to-noise ratio.

Potential improvements are the application of another Fourier window to better diffuse the energy between the frequency bands and the use of other iterative methods to calculate the deconvolution solution.

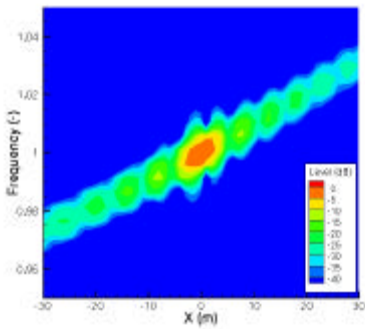
REFERENCES

- [1] S. R. Venkatesh, D.R. Polak and S. Narayanan, "Beamforming algorithm for distributed source localization and its application to jet noise," *AIAA Journal* 41(7), 1238-1246, 2003.
- [2] J-F. Piet and G. Elias, "Airframe noise source localization using a microphone array," 3rd AIAA/CEAS Aeroacoustics Conference, Atlanta, GA (USA), 12-14 May 1997, AIAA-1997-1643.
- [3] U. Michel and P. Böhning, "Investigation of aircraft wake vortices with phased microphone arrays," 8th AIAA/CEAS Aeroacoustics Conference, Breckenridge, Colorado (USA), 17-19 June 2002, AIAA-2002-2501.
- [4] C. Lewis and P. Joseph, "A focused beamformer technique for separating rotor and statot-based broadband sources," 12th AIAA/CEAS Aeroacoustics Conference, Cambridge, Massachusetts (USA), 8-10 May 2006, AIAA-2006-2710.
- [5] J. Piet, U. Michel and P. Böhning, "Localization of the acoustic sources of the A340 with a large microphone array during flight tests," 8th AIAA/CEAS Aeroacoustics Conference, Breckenridge, Colorado (USA), 17-19 June 2002, AIAA-2002-2506.
- [6] T. Brooks and W. Humphreys, "A deconvolution approach for the mapping of acoustic sources (DAMAS) determined from phased microphone array," *J. Sound and Vibr.* 294(4-5), 856-879, 2006.
- [7] D. Blacodon, "Spectral analysis of airframe noise of an aircraft model A320/A321," 11th AIAA/CEAS Aeroacoustics Conference, Monterey, California (USA), 23-25 May 2005, AIAA-2005-2809.
- [8] S. Brühl and A. Röder, "Acoustic noise source modelling based on microphone array measurements," *J. Sound and Vibr.* 231(3), 611-617, 2000.
- [9] R. P. Dougherty, "Extensions of DAMAS and benefits and limitations of deconvolution in beamforming," 11th AIAA/CEAS Aeroacoustics Conference, Monterey, California (USA), 23-25 May 2005, AIAA-2005-2961.

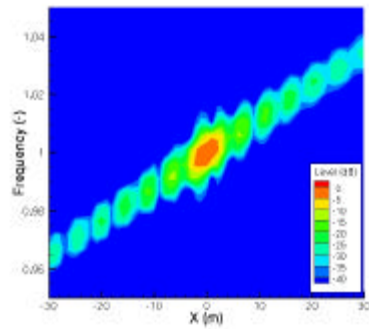
- [10] K. Ehrenfried and L. Koop, “A comparison of iterative deconvolution algorithms for the mapping of acoustic sources,” 12th AIAA/CEAS Aeroacoustics Conference, Cambridge, Massachusetts (USA), 8-10 May 2006, AIAA-2006-2711.
- [11] S. Guérin, U. Michel, H. Siller, U. Finke and G. Saueressig , “Airbus A319 database from dedicated flyover measurements to investigate noise abatements procedures,” 11th AIAA/CEAS Aeroacoustics Conference, Monterey, California (USA), 23-25 May 2005, AIAA-2005-2981.
- [12] S. Guérin and U. Michel, “Aero-engine noise investigated from flight tests,” 12th AIAA/CEAS Aeroacoustics Conference, Cambridge, Massachusetts (USA), 8-10 May 2006, AIAA-2006-2463.



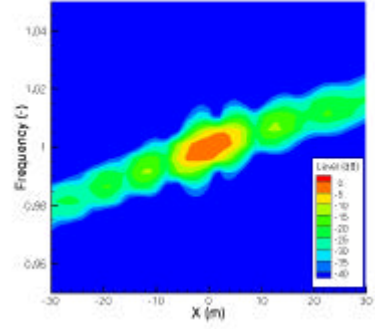
a) $U=0$ m/s, $q=90^\circ$



b) $U=80$ m/s, $q=60^\circ$



c) $U=80$ m/s, $q=90^\circ$



d) $U=80$ m/s, $q=120^\circ$

Fig. 1. Beamforming pattern for a) static point source ($U=0$ m/s, altitude 200 m), b), c) and d) a moving point source ($U=80$ m/s, altitude 200 m). Simulations performed with a harmonic source at 1 kHz and a line array of 101 microphones with 15 m aperture.

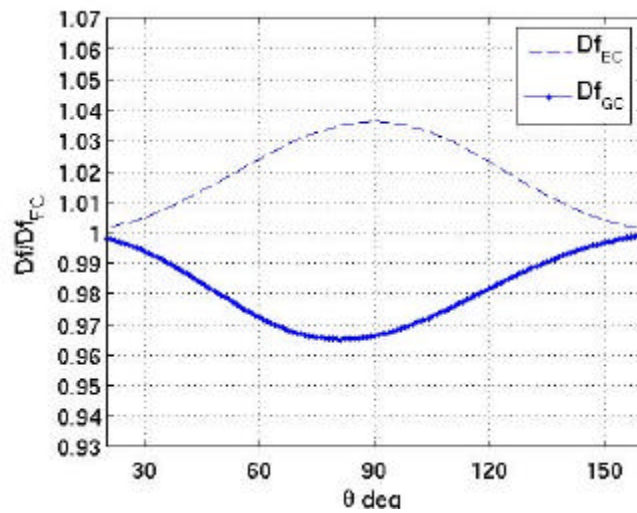


Fig. 2. Doppler factor variations of the side-lobes at the limits of the map area for a source moving with a speed of 80 m/s at 200 m altitude.

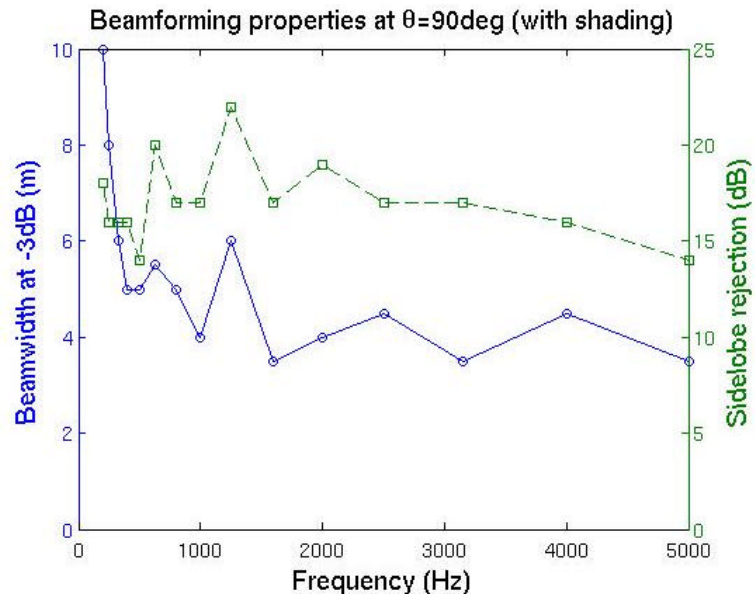


Fig. 3. Beamforming properties at 90° for the spiral array used in the simulations (altitude, 200m).

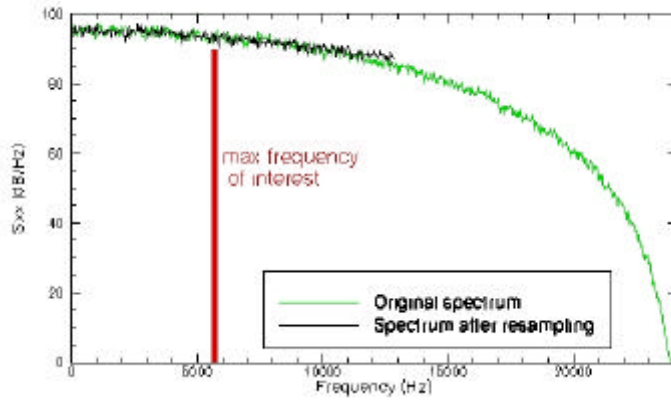


Fig. 4. Spectrum of a simulated broadband point source.

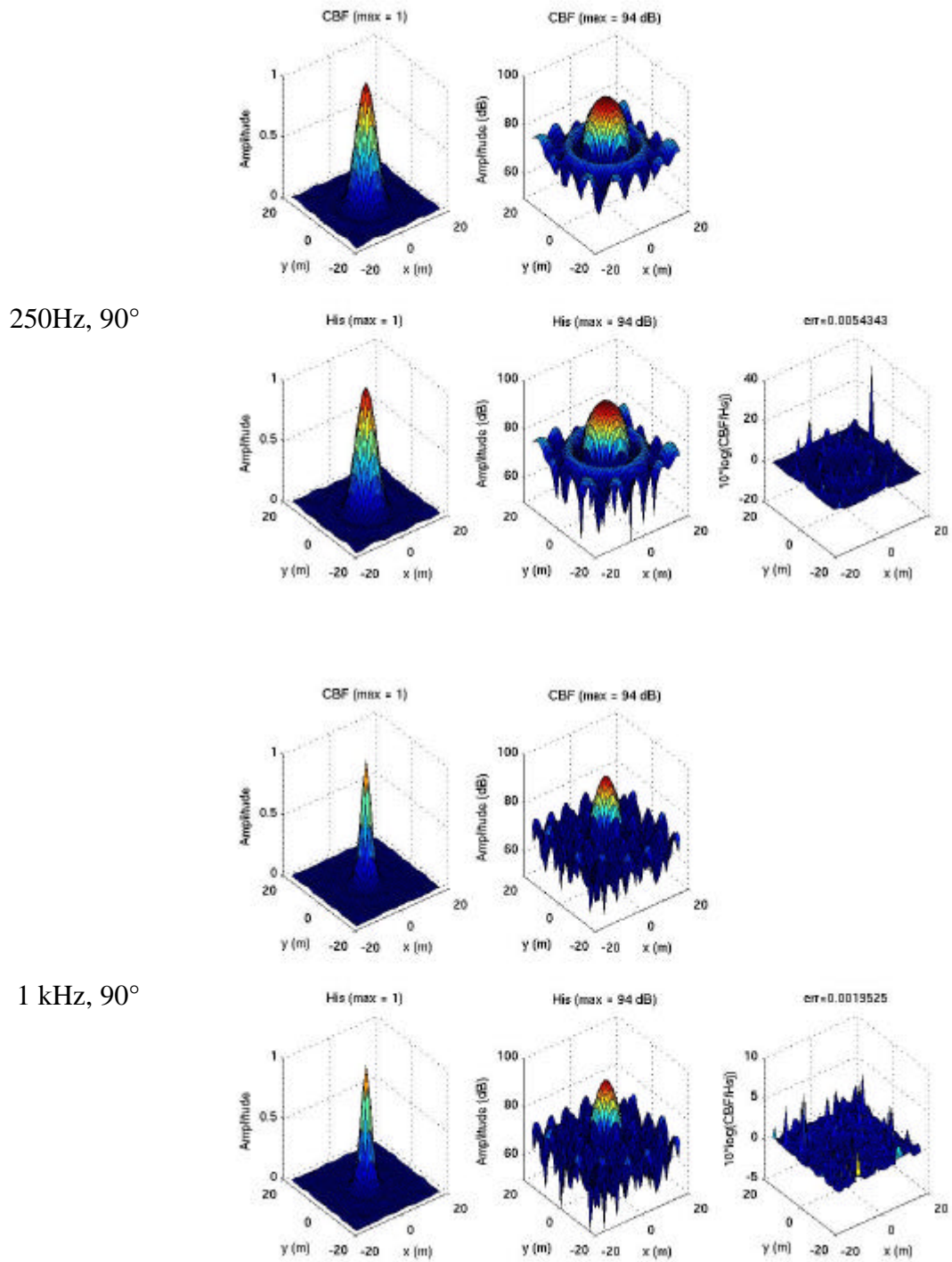


Fig. 5. Time domain beamforming (top sub figures) vs point spread function (bottom left figures) and difference (bottom right figure) (S1, $U=0.1$ m/s).

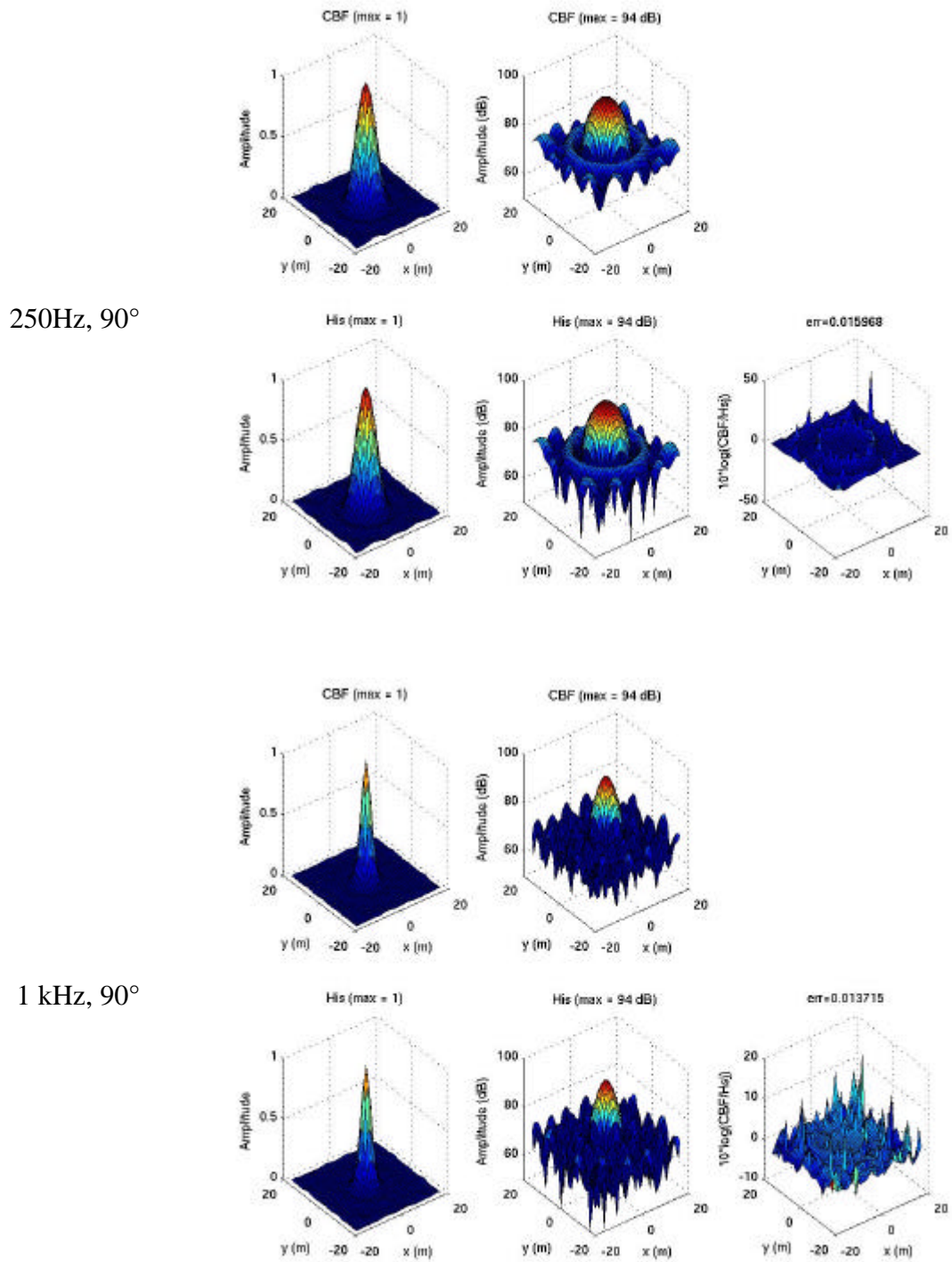


Fig. 6. Time domain beamforming (top figures) vs point spread function (bottom left figures) and difference (bottom right figure) (SIM, $U=80$ m/s).

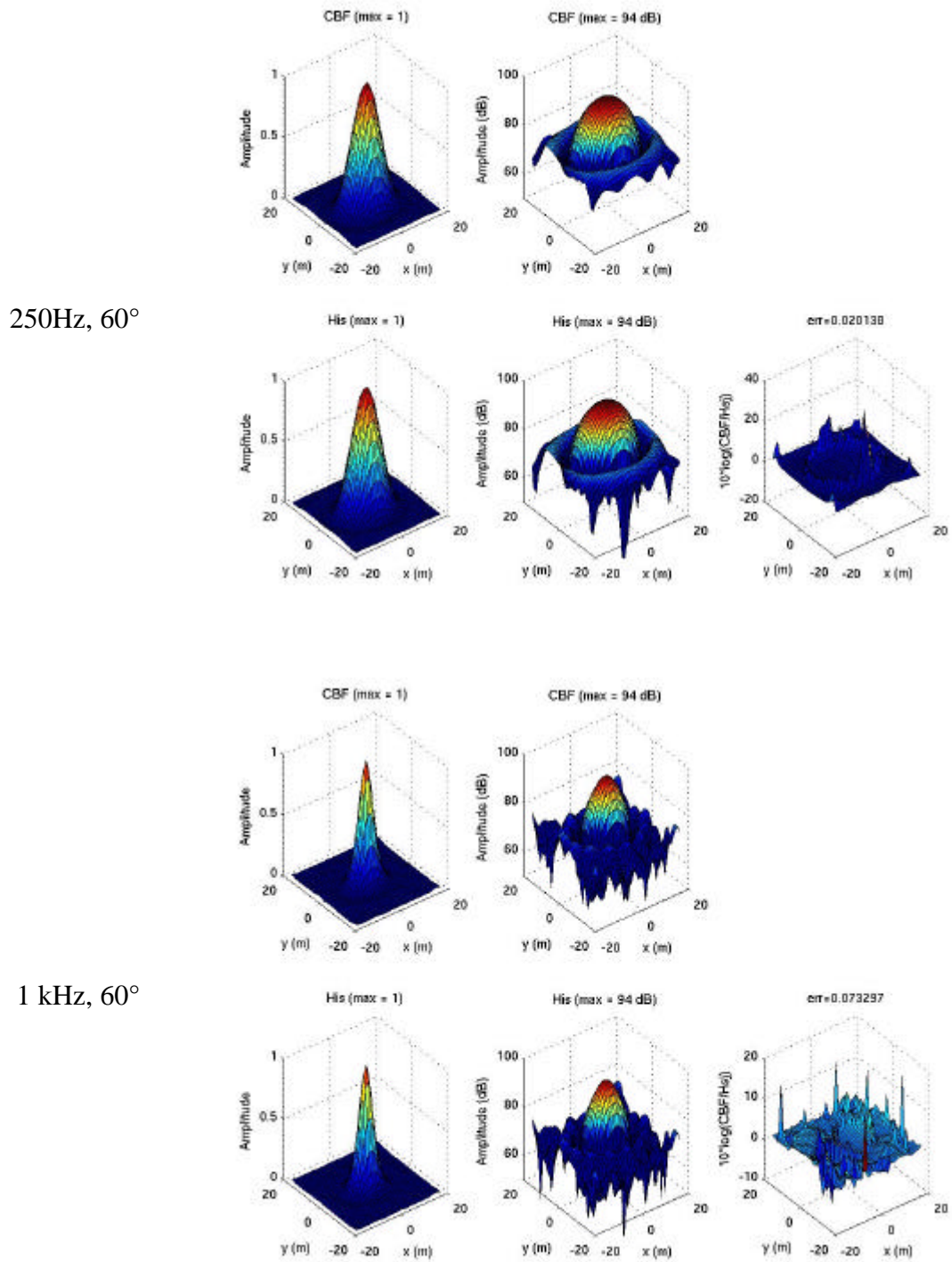


Fig. 7. Time domain beamforming (top figures) vs point spread function (bottom left figures) and difference (bottom right figure) for emission angle 60° (S1, U=0.1 m/s).

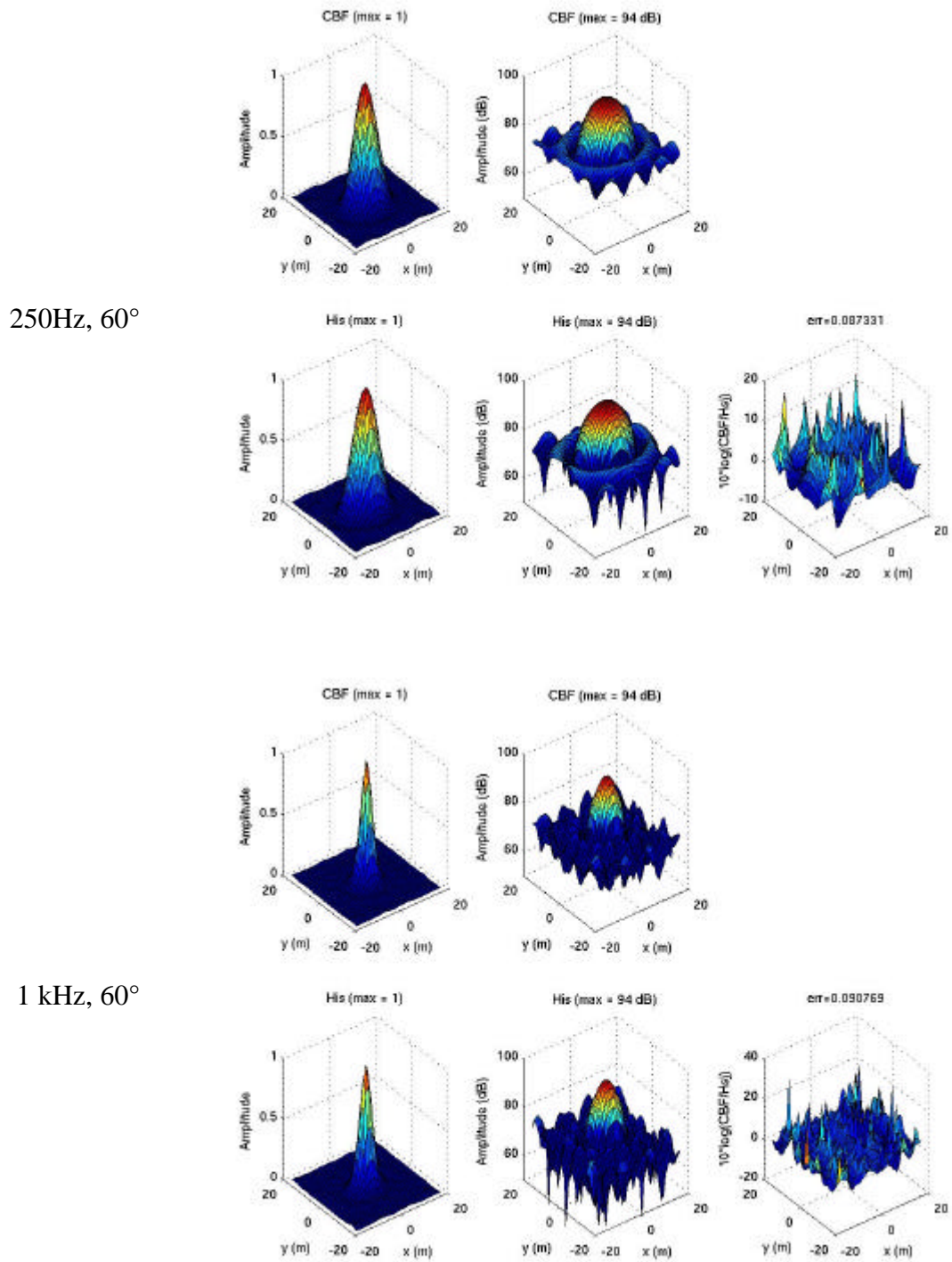


Fig. 8. Time domain beamforming (top figures) vs point spread function (bottom left figures) and difference (bottom right figure) for emission angle 60° (SIM, $U=80$ m/s).

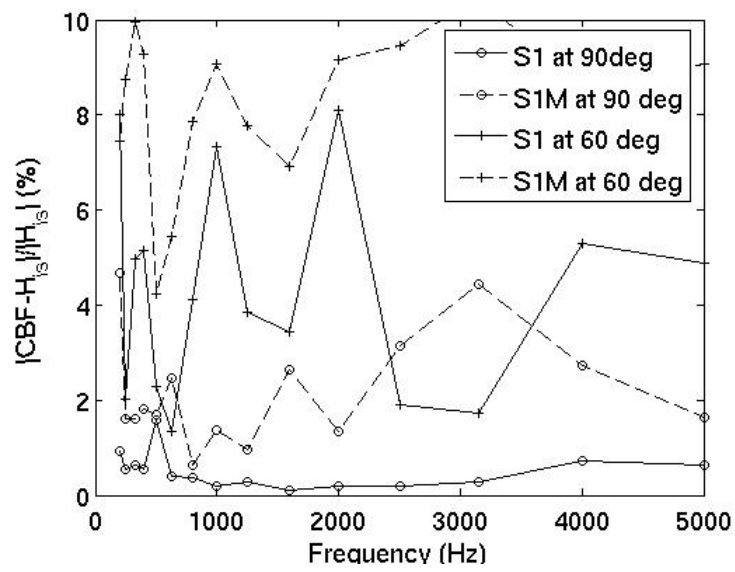


Fig. 9. Difference between the time domain beamforming solution and the modelled point spread function. This error was calculated for a 37×37 mesh with 1 m grid spacing.

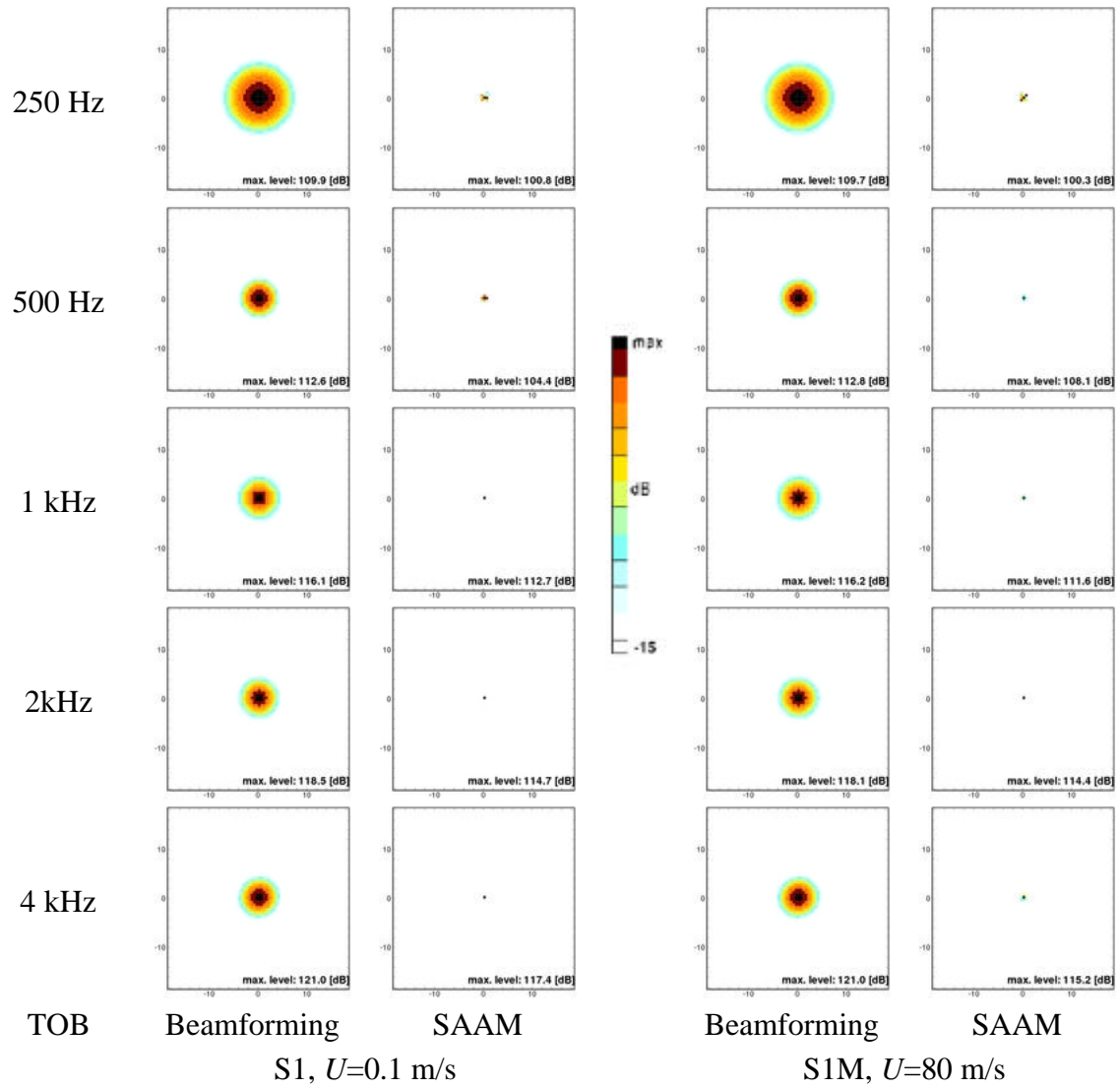


Fig. 10. Beamforming maps in comparison with the results of the deconvolution at 90° in one-third octave bands.

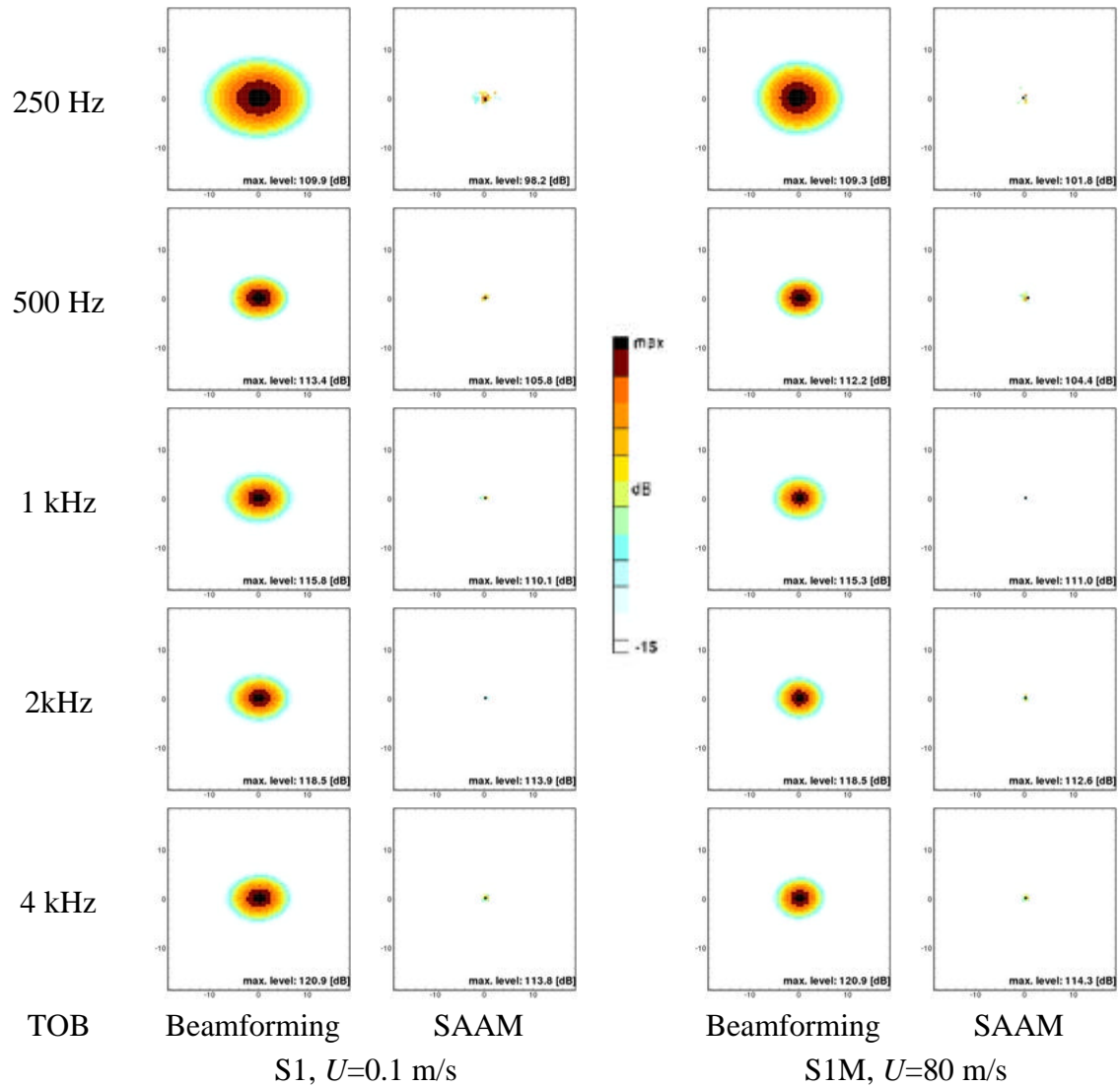


Fig. 11. Beamforming maps in comparison with the results of the deconvolution at 60° in one-third octave bands.

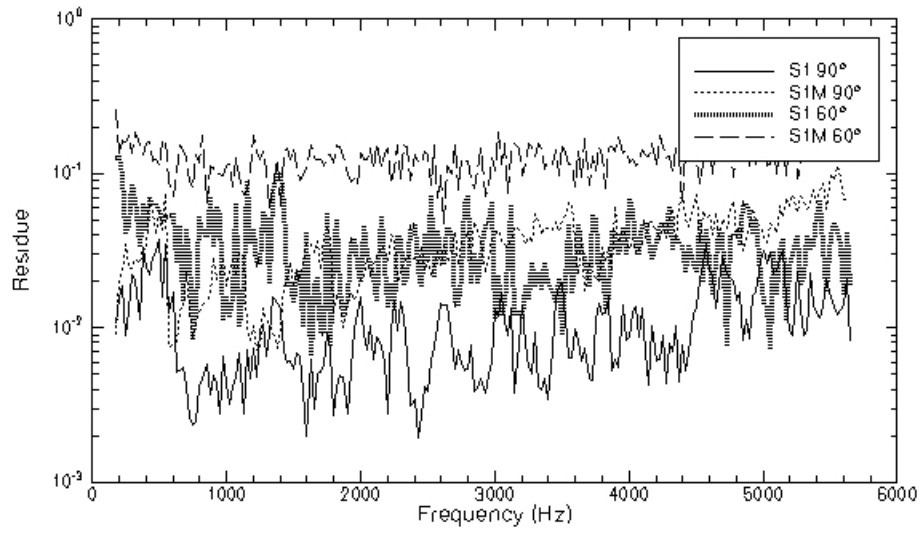


Fig. 12. Normalized residual.

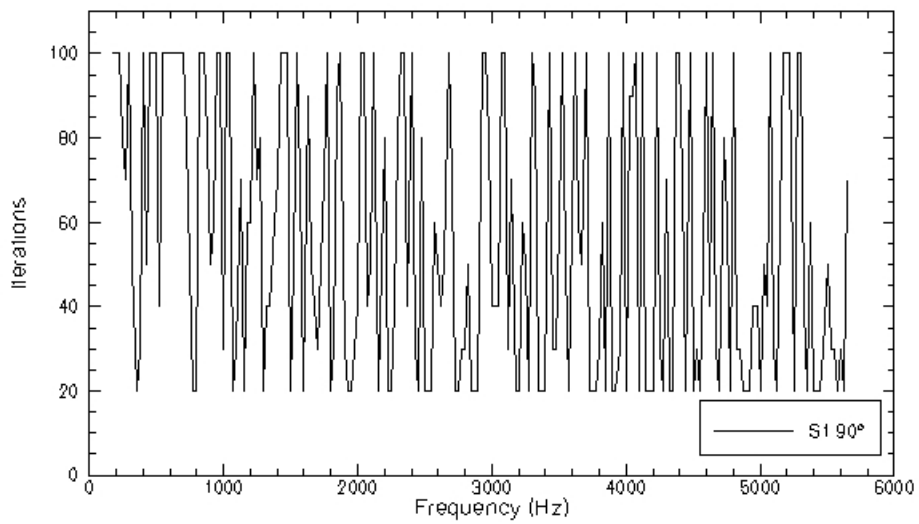


Fig. 13. Number of iterations for each frequency band.

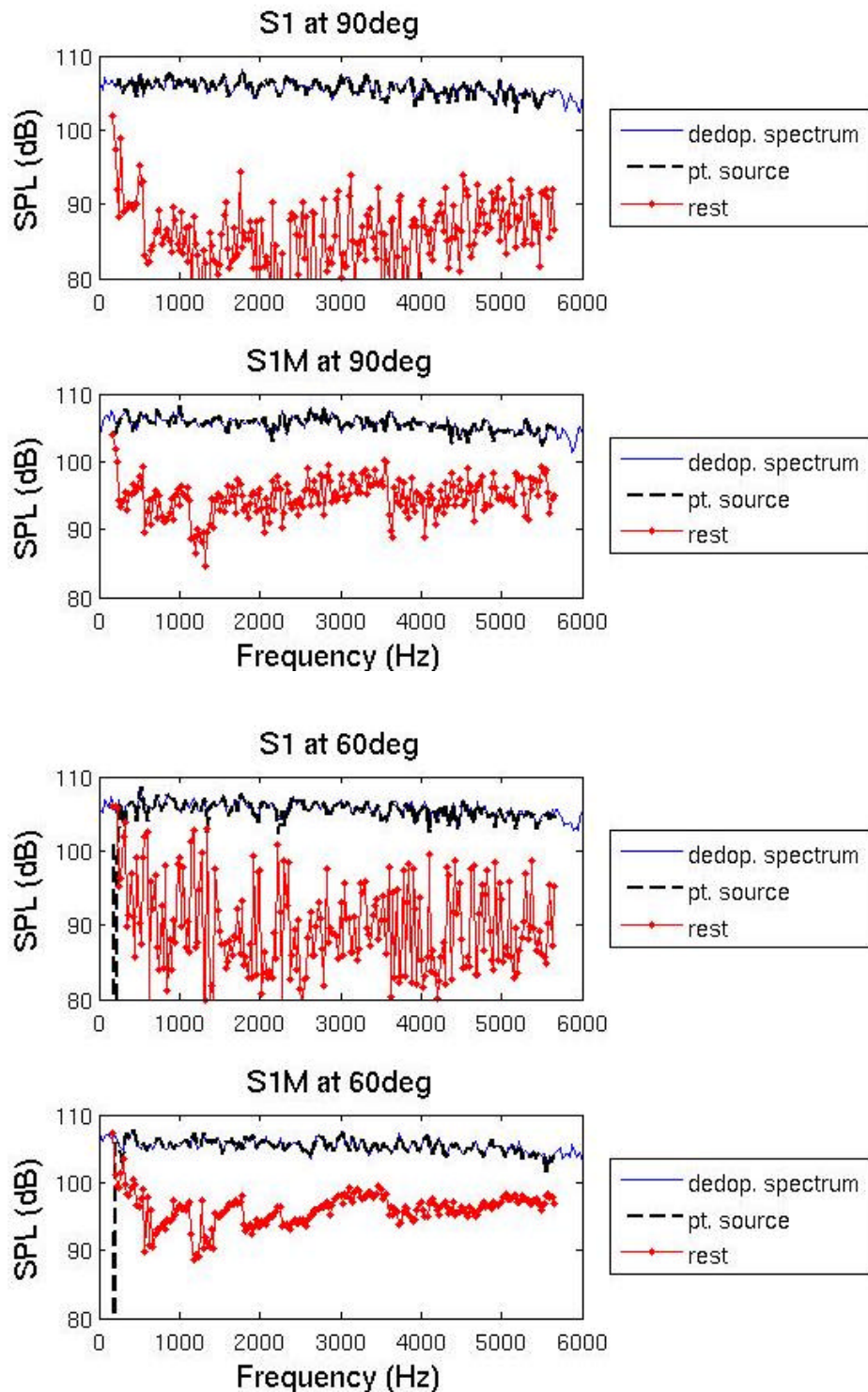


Fig. 14. Comparison between the original source spectrum and the reconstructed one for the test cases S1 and S1M.

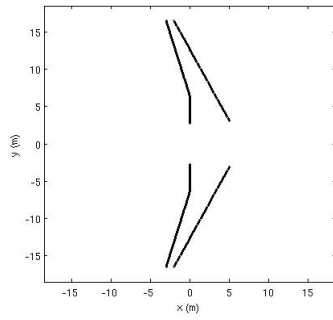


Fig. 15. Source position for the test case S5.

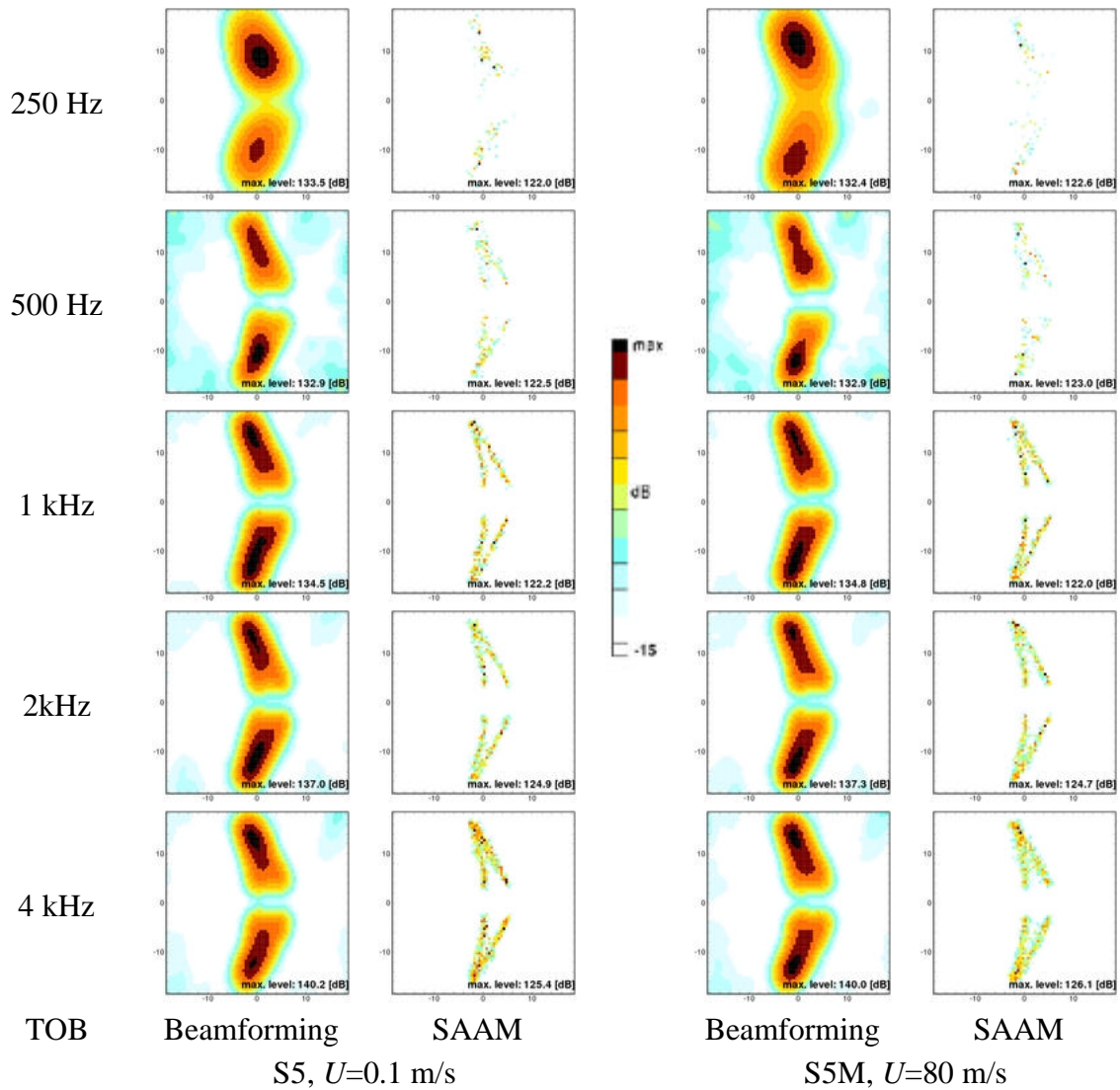


Fig. 16. Beamforming maps in comparison with the results of the deconvolution at 90° in one-third octave bands.

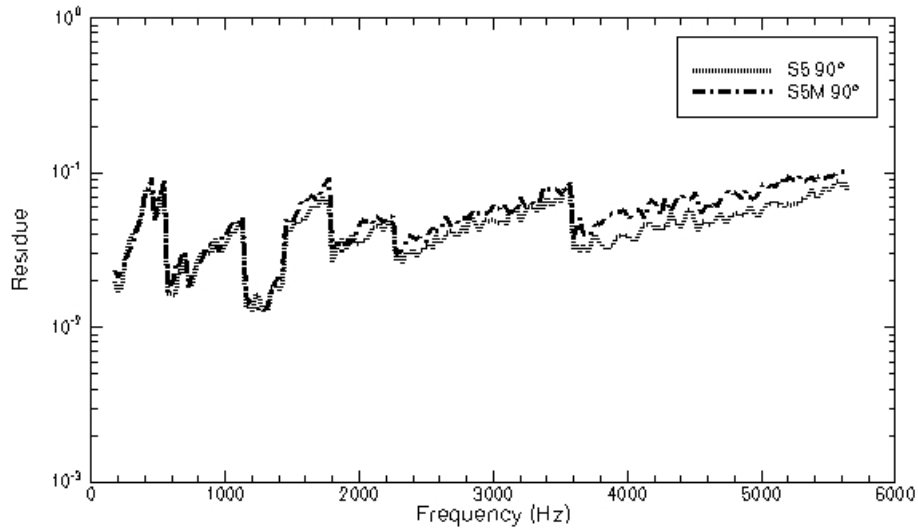


Fig. 17. Normalized residual.

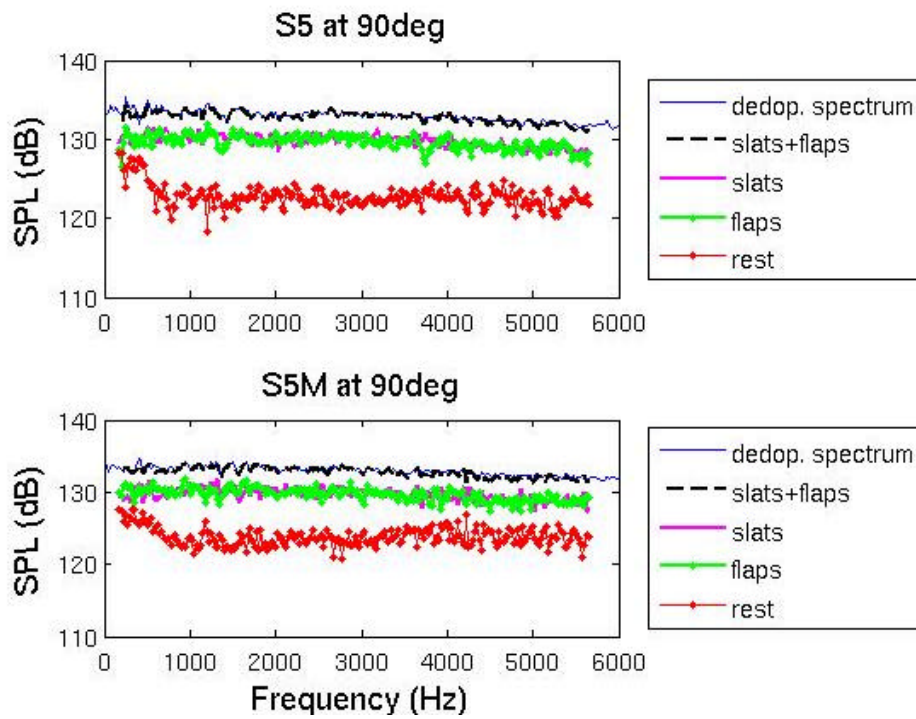


Fig. 18. Comparison between the original source spectrum and the reconstructed one for the test cases S5 and S5M.

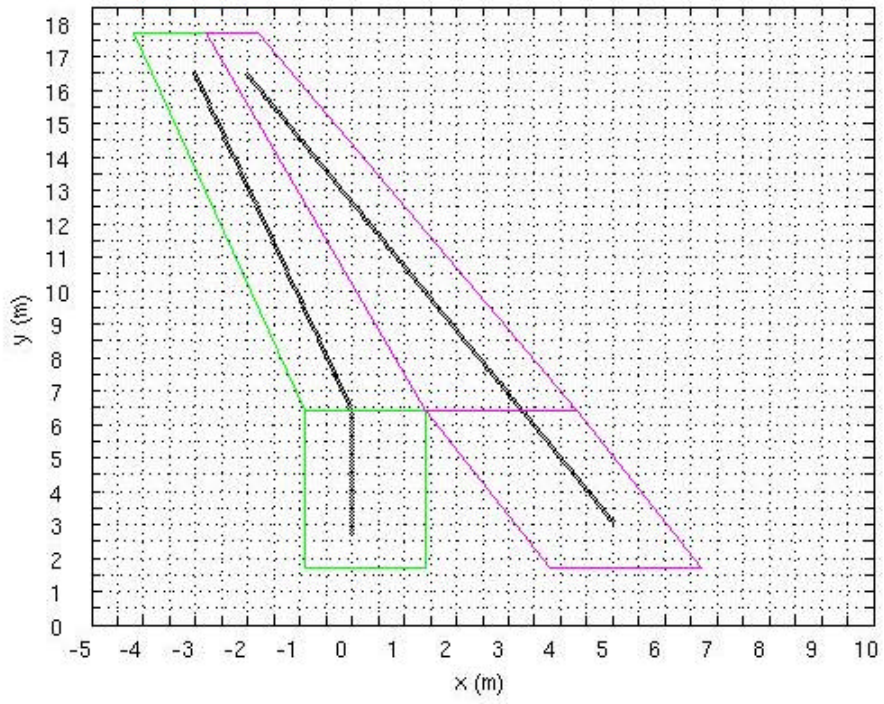


Fig. 19. Integration surfaces.